Asian Journal of Chemistry; Vol. 37, No. 11 (2025), 2703-2711
ASIAN JOURNAL OF CHEMISTRY
https://doi.org/10.14233/ajchem.2025.34553

Self-Organization of Nanostructured Cadmium Selenide Nanorods by Electrophoretic Deposition Technique

R. YOGA INDRA ENIYA, K. VIJAYKUMAR and B. VIGNEASHWARI*

Department of Physics, Government Arts College for Men, Krishnagiri- 635002, India

*Corresponding author: E-mail: vigneashwari@gmail.com

Received: 28 July 2025 *Accepted*: 11 September 2025 *Published online*: 27 October 2025 AJC-22157

In this work, nanocrystals (~76.6 nm) of semiconducting CdSe, obtained through chemical synthesis using a hydrothermal method, were analyzed for their structural and optical properties and compositional purity. These CdSe NRs were electrically driven from a monodisperse colloidal suspension onto a transparent conducting indium tin oxide (ITO) substrate by the electrophoretic deposition (EPD) method and nanostructured thin films were obtained. The interesting morphologies were observed by controlling the deposition parameters on the cluster growth of CdSe. Optical microscopy and SEM analysis revealed an organized nanorods assembly driven by the applied electric field. The resulting films retained their crystallinity and phase purity, confirming the eco-friendly and cost-effective nature of the EPD method. These structured CdSe assemblies show strong potential for photovoltaic and sensor applications.

Keywords: Cadmium Selenide, Charge driven nanoparticles, Electrophoretic deposition, Self-organization, Deposits.

INTRODUCTION

The II–VI semiconductor compounds, particularly selenides, are widely studied for their enhanced physico-chemical properties, making them suitable for applications in sensors, photovoltaics, energy storage and optoelectronic devices [1,2]. Nanostructured forms of these materials exhibit size-dependent behaviour and can be assembled into nano- and microscale architectures, offering improved performance in the functional materials, device integration, *etc.* [3-6]. Selenide-based semiconducting nanoparticles are attracting several researchers due to their brilliant prospects. Especially, cadmium selenide (CdSe) has garnered significant interest due to its wide range of applications in applied physics and materials science [7-10]. CdSe is an n-type semiconductor that has ingenious behaviour and crystallizes into three different crystal structures such as wurtzite (hexagonal), rock salt (cubic) and sphalerite (cubic), with a direct band gap of 1.74 eV at ambient conditions [11-14].

For device-level applications, assembling CdSe nanoparticles into aggregated nanostructures is essential. Nanostructured films offer significantly higher surface area than their bulk counterparts, which is critical for enhancing performance in catalysis, photoelectrochemical cells and sensor applications, where efficiency or sensitivity scales with surface area [15]. Various thin-film deposition techniques have been employed for CdSe growth, including vacuum-based methods such as physical vapor deposition (PVD) and chemical vapor deposition (CVD), though these often suffer from high defect densities and broad particle size distributions. While advanced methods like molecular beam epitaxy (MBE), magnetron sputtering and pulsed laser deposition (PLD) offer improved control, they are typically cost-effective [16,17].

Unlike vapor-phase methods, EPD enables rapid film formation without complex equipment or environmental hazardousness. The process relies on the electrophoretic mobility of charged particles in a suspension, which are deposited onto an oppositely charged electrode under a DC electric field [18-22]. The only disadvantage of EPD as compared with dip and slurry coating is the incompatibility with water as a suspension medium, due to gas evolution (H_2 and O_2) under applied voltage, which compromises the quality of film. Successful EPD requires a stable, homogeneous suspension of well-dispersed, small sized particles to avoid sedimentation and ensure uniform deposition. The electrophoretic mobility of charged particles must exceed gravitational settling and high, uniform surface charge on particles is essential. Stability in suspension is governed by the balance between electrostatic repulsion and van der Waals attraction, with surface charge building at the

solid-liquid interface [23]. Particles smaller than 1 μm remain suspended due to Brownian motion, while larger particles require continuous agitation. The quality and morphology of the deposited film depend on multiple, interrelated parameters influencing EPD kinetics [24].

In this work, the CdSe NRs were synthesized by hydrothermal method and deposited electrophoretically on transparent conducting ITO substrates, which were characterized for structural, optical, compositional properties and surface morphology. The comparison between powder CdSe and as-deposited film was investigated by fixing the deposition voltage (30 V) and distance between the electrodes (3 mm). The formation of nanorods into self-organized fractals was observed under EPD. In the present work, electrophoretic deposition was performed without any complexing agents, templates, binders and any post-treatment procedures. This study comprises of developing a nanostructured assembly of CdSe NRs under the applied electric field.

EXPERIMENTAL

Synthesis of CdSe nanorods: All the chemicals used in this experiment were of analytical grade (AR), which were purchased from Merck company and used without any further purification. CdSe NRs were synthesized using cadmium chloride monohydrate ($CdCl_2 \cdot H_2O$), aqueous ammonia ($NH_3 \cdot H_2O$), selenium metal powder and sodium sulphite. In brief, 1 M of $CdCl_2 \cdot H_2O$ was dissolved in 70 mL deionized water (DIW) and stirred for 30 min. The ammonia solution was added slowly until the pH~12 is achieved. Furthermore, 60 mL of freshly prepared solution of Na_2SeSO_3 (0.8 M) was added dropwise until solution becomes homogenous and stirred magnetically for 1 h. Then, the resulted mixture was transferred into the Teflon-lined stainless-steel autoclave for hydrothermal process to take place. The autoclave was sealed and kept in the hot air oven at 150 ºC for 16 h. The resulted black powders were washed and centrifuged multiple times with deionized water followed by ethanol and finally dried at 70 ºC for 5 h in vacuum oven.

Electrophoretic deposition (EPD) of CdSe: The experimental setup was constructed with a DC voltage supply, with an EPD cell comprising of two electrodes which was separated by a spacer made of Teflon block. A conducting indium tin oxide (ITO)-coated glass was used as a working electrode whereas counter electrode was made of stainless-steel plate and were mounted vertically in EPD cell. A colloidal suspension was prepared by dispersing 0.5 g of as-synthesized CdSe NRs in 10 mL of propylene carbonate, which served as suspension medium. The mixture was subjected to ultrasonication to ensure uniform dispersion of individual nanoparticles and to break apart any agglomerates. The resulting suspension was stable and well-dispersed. Suspension stability plays a critical role in determining the quality and uniformity of the deposited films [25]. In this study, the suspension concentration and deposition voltage were optimized through the preliminary trial experiments. The electrode spacing was fixed at 3 mm and a constant potential of 30 V was applied. Deposition time was systematically varied between 120 s and 300 s to assess its effect on film morphology and coverage. Following deposition, the films were allowed to dry under ambient conditions. A uniform, adherent black film was consistently deposited on the cathodic surface of the ITO-coated glass substrate, confirming effective electrophoretic deposition.

Characterization: XRD of CdSe powder was performed with Cu*K*α radiation in powder (PXRD) and for deposits, grazing incidence (GIXRD) modes using Bruker AXS D2 phaser X-ray diffractometer and Bruker D8 Advance in Bragg-Brentano geometry, at 0.5º as grazing incidence angle. Optical absorption of CdSe powder was recorded using UV-DRS analysis in UV-visible region using Jasco-UV-vis-NIR (V-770, Serial No. A012061801) spectrophotometer. The optical microscopy analysis was performed to investigate about the information of deposits at microlevel using Weswox optical microscope. The surface morphology of CdSe powder was analyzed using Carl ZEISS-SIGMA 300 FESEM with EDAX. The self-organization and elemental composition of CdSe films were examined with scanning electron microscope (SEM) and EDAX by using Carl ZEISS (Germany) microscope Model: GmbH – EVO 18.

RESULTS AND DISCUSSION

X-ray diffraction studies: The PXRD profile of the as-synthesized CdSe powder and the GIXRD pattern of the electrophoretically deposited film (Fig. 1) confirm the crystallization in the hexagonal wurtzite phase of CdSe, consistent with the standard diffraction pattern reported in JCPDS card No. 77-0046. The powder X-ray diffraction (PXRD) pattern of the as-synthesized CdSe powder exhibits an abnormally high intensity for the (100) reflection, suggesting a preferential orientation or anisotropic crystal convention. This feature is absent in the PXRD pattern of the CdSe thin film, indicating a loss of such orientation during film formation. The sharp and well-defined diffraction peaks of the powder sample, with no detectable secondary phases, confirm its phase purity and high crystallinity. In contrast, the broadening of diffraction peaks in the film indicates the retention of nanocrystalline characteristics following electrophoretic deposition. The GIXRD analysis further confirms that the deposited CdSe film is phase-pure, nanocrystalline in nature and adopts a hexagonal crystal structure, with no evidence of impurity phases. However, the signature peaks of ITO substrates could be clearly observed. The lattice dimensions and lattice parameters were calculated using UNITCELL program software [26] and calculated values are presented in Table-1. For both powder and film the lattice dimensions were obtained at $\alpha = \beta = 90^\circ$ and $\gamma = 120^\circ$. The unit cell volume and lattice parameters of CdSe were found to increase due to lattice expansion during EPD onto the ITO substrate [27]. A visible reduction in the diffraction peak intensities was observed in the CdSe film, indicating changes in crystallinity. To provide a clearer analysis, zoomed-in views of the (100), (002) and (101) planes are shown in Fig. 2. Moreover, a decrease in the degree of crystallinity and a pronounced peak shift of the (100) plane toward lower angles (Fig. 3) suggest the presence of lattice strain and changes in crystallite size induced by the EPD process.

The Debye-Scherrer equation was used to calculate the average crystallite size. While the pristine CdSe powder exhi-

TABLE-1
XRD PARAMETERS VALUES OF CdSe POWDER AND DEPOSIT

Test conditions	Lattice parameters a = b ≠ c (Å)	Unit cell volume (Å^3)	Crystallite size (D)	d-spacing (Å) of (100) plane
CdSe powder	4.307, 7.010	112.53	76.6 nm	3.715
CdSe deposit	4.310, 7.012	112.82	30.0 nm	3.742

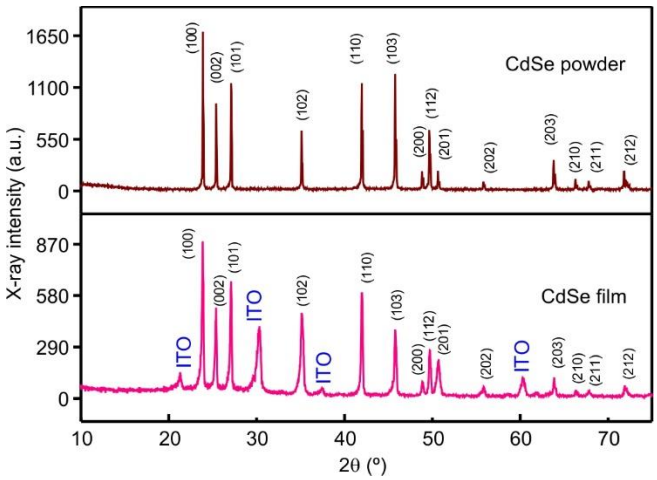

Fig. 1. XRD spectra of (a) CdSe powder and CdSe-deposit

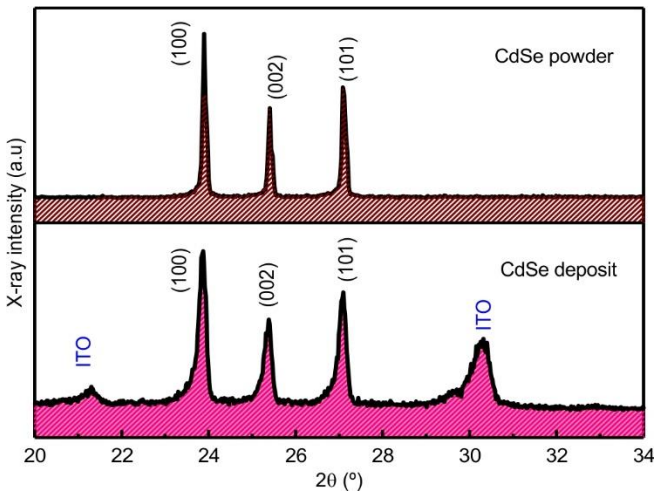

Fig. 2. XRD spectra of zoomed-in version of (100), (002), (101) planes of CdSe powder and deposit

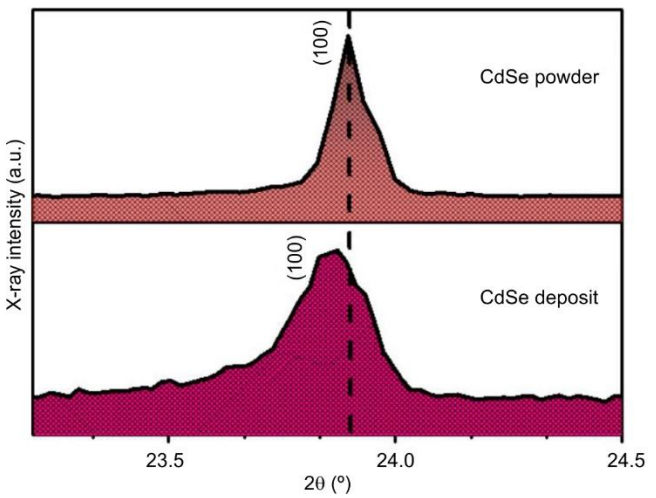

Fig. 3. Magnified XRD spectra version of (100) plane of CdSe powder *versus* deposit

bited a crystallite size of approximately 76.5 nm, the EPD-deposited CdSe film showed a reduced average crystallite size of 30 nm. This variation is attributed to the influence of the applied electric field on grain boundaries, which can promote grain fusion or fragmentation, resulting in non-uniform crystallite sizes. Moreover, during sample preparation, the CdSe colloidal suspension was ultrasonicated and the decanted solution, containing smaller nanoparticles, was used for deposition. This process inherently favours the deposition of finer particles, as larger particles tend to settle due to gravity [15,23]. Consequently, the CdSe film exhibits a smaller crystallite size than the original powder.

Fig. 4 presents the variation of crystallite size as a function of lattice strain for both the CdSe powder and the electrophoretically deposited film. The hexagonal wurtzite structure is retained in the deposited film, indicating structural stability under the influence of the EPD process. This structural preservation can be attributed to the inherent nature of CdSe, where covalently bonded Cd and Se atoms are arranged in a Se-Cd-Se-Cd sequence and are held together by relatively weak van der Waals interactions between layers. Fig. 5 shows the hexagonal structure of CdSe, where, Se^{2-} anions form a covalent bond and get combined with Cd^{2+} cations. Each Cd^{2+} is bonded to four Se^{2-} atoms. In powder CdSe, it could be observed the plane (110) and (103) shows the slight split in peak (shoulder peak), which appears converged in CdSe film. In powder CdSe, the shoulder peaks might be due to the distortions in the lattice, the structural imperfections and asymmetrical orientation of Cd atoms around Se atoms. But, in CdSe film, the shoulder peaks got merged with the main diffraction planes (110) and (103) and those planes becomes more ordered as compared to CdSe powder (Fig. 6). The broadening of diffraction peaks in CdSe film might be due to lattice expansion [28] under the impact of deposition voltage (30 V). The interplanar spacing (*d*-spacing) of CdSe films were tend to increase as compared to CdSe powder. This observation indicates a slight upward shift in the lattice planes, suggesting an expansion in lattice parameters. Consequently, this results in an increase in the unit cell volume, confirming the occurrence of lattice expansion [29,30]. Fitzpatrick *et al*. [31] stated that the regular strain causes either contraction or expansion to the unit cell, which causes the shifting of diffraction peaks without broadening the peaks.

Contrarily, the slight peak shifting from the original positions of atoms and peak broadening was also observed in CdSe film, which might be due to the reduction in the average crystallite size and irregular lattice strain [32] aroused by EPD of CdSe. Such kind of irregular lattice strains might be due to the existence of many defects within the crystal lattice such as point defects, plastic deformation and reduced degree of crystallinity of the material. Plastic deformation has been observed in halide single crystals under the influence of an applied electric field [33]. The obtained results show that the

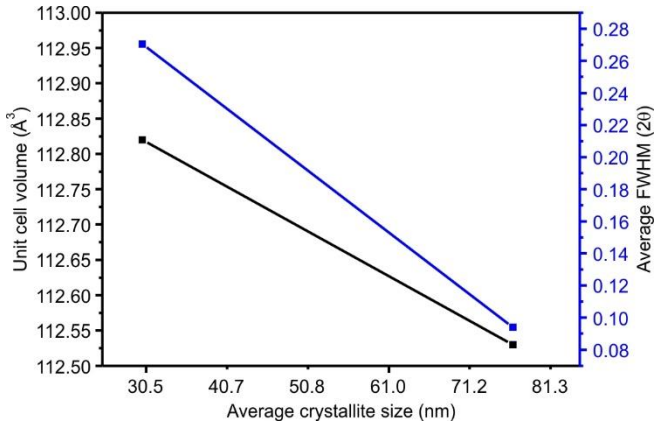

Fig. 4. Variation plot of unit cell volume and FWHM against the average crystallite size of CdSe powder and deposit

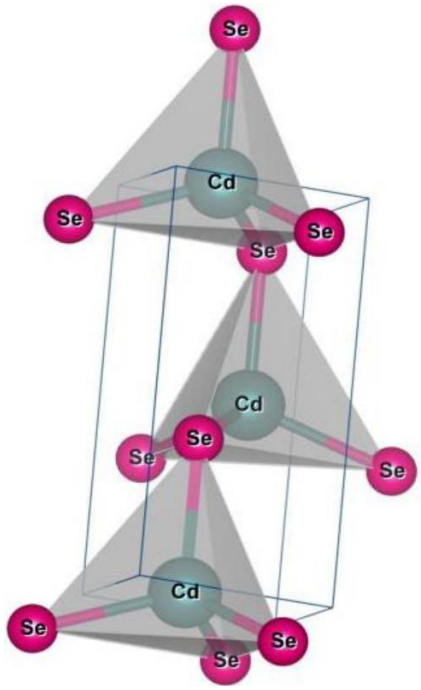

Fig. 5. Hexagonal (wurtzite) structure of cadmium selenide nanorods

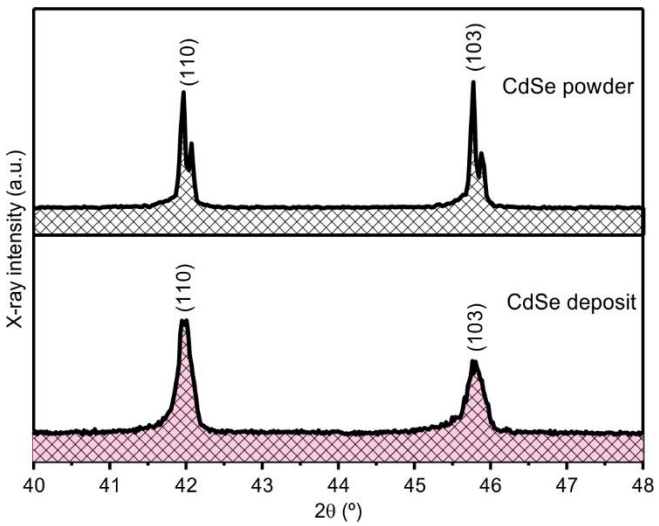

Fig. 6. XRD patterns of zoomed-in planes of (110) and (103) for CdSe powder and deposit

lattice expansion makes the bonds between CdSe to expand and the influence of electric field repositions the atoms from their original place during the film growth.

FESEM micrograph of CdSe powder nanoparticles for investigating the microstructure displayed in Fig. 7a-d and the EDAX spectrum for analysing the compositional purity are displayed in Fig. 8. FESEM image shows an irregular morphology with huge population of flaky nanorods and fewer nanospheres with larger diameter. The obtained results corroborate with PXRD analysis. The length and diameter of CdSe nanorods were calculated using ImageJ software. The CdSe nanorods were 200 nm in length and 30 nm to 50 nm in diameter and is apparently shown in Fig. 7c-d.

The elemental composition of CdSe powder was obtained with SEM/EDAX. The peaks associated with cadmium (Cd) and selenium (Se) elements could be seen in the host material of CdSe nanorods where other peaks were due to specimen grid during the data acquisition. The atomic weight percentage of Cd and Se in EDAX spectrum clearly indicates the formation of pure-CdSe without any impurities. Also, it indicates Cd:Se in the ratio of 1:1

Optical characterization of powder-CdSe: The optical properties for nanocrystalline CdSe powder were recorded in UV-vis region within the range of 350 to 850 nm is shown in Fig. 9. The absorption edge was estimated at 718 nm and it attributes a band gap of 1.72 eV to CdSe powder sample. Such a bandgap might be due to length of the nanorods as measured in FESEM was found to be 200 nm and diameter of 30 to 50 nm, respectively. According to Hegazy *et al*. [34], the band gap of CdSe NRs are size-dependent, then the energy band gap could be described using the following relation:

$$E_g = h\nu = \frac{hc}{\lambda_{max}}$$

where E_g denotes the energy band gap of CdSe NRs; h is the Planck's constant (6.626×10^{-34} Js); c is the velocity of light (3×10^8 m/s).

It indicates a red shift in absorption wavelength as compared to bulk CdSe of wurtzite structure (λ_{max} = 716 nm, E_g = 1.76 eV). Other reports of such optical properties of similar bandgap values are also reported in the literature [35,36].

Optical microscope image of deposits: Fig. 10 represents the optical micrographs of CdSe deposited at different durations was obtained using a Weswox optical microscope. The presented micrographs were recorded with same magnification at centre of bare ITO substrate and deposited CdSe films after drying it naturally where the parameters such as deposition voltage and separation between the electrodes were fixed to investigate about the rate of deposition by varying the deposition duration. The deposited films at t_d = 120 s and 300 s is named as sample A and B, respectively. At 120 s, the formation crack-free deposit could be seen and the surface coverage was minimal with.

But when deposition duration was increased to 300 s, best surface coverage was achieved and interestingly development of cracks along with the delamination process started and grouping of islands like fractal structures in between the cracks at micrometre range could be observed. Similar reports of crack formation and delamination of CdSe deposit were obtained

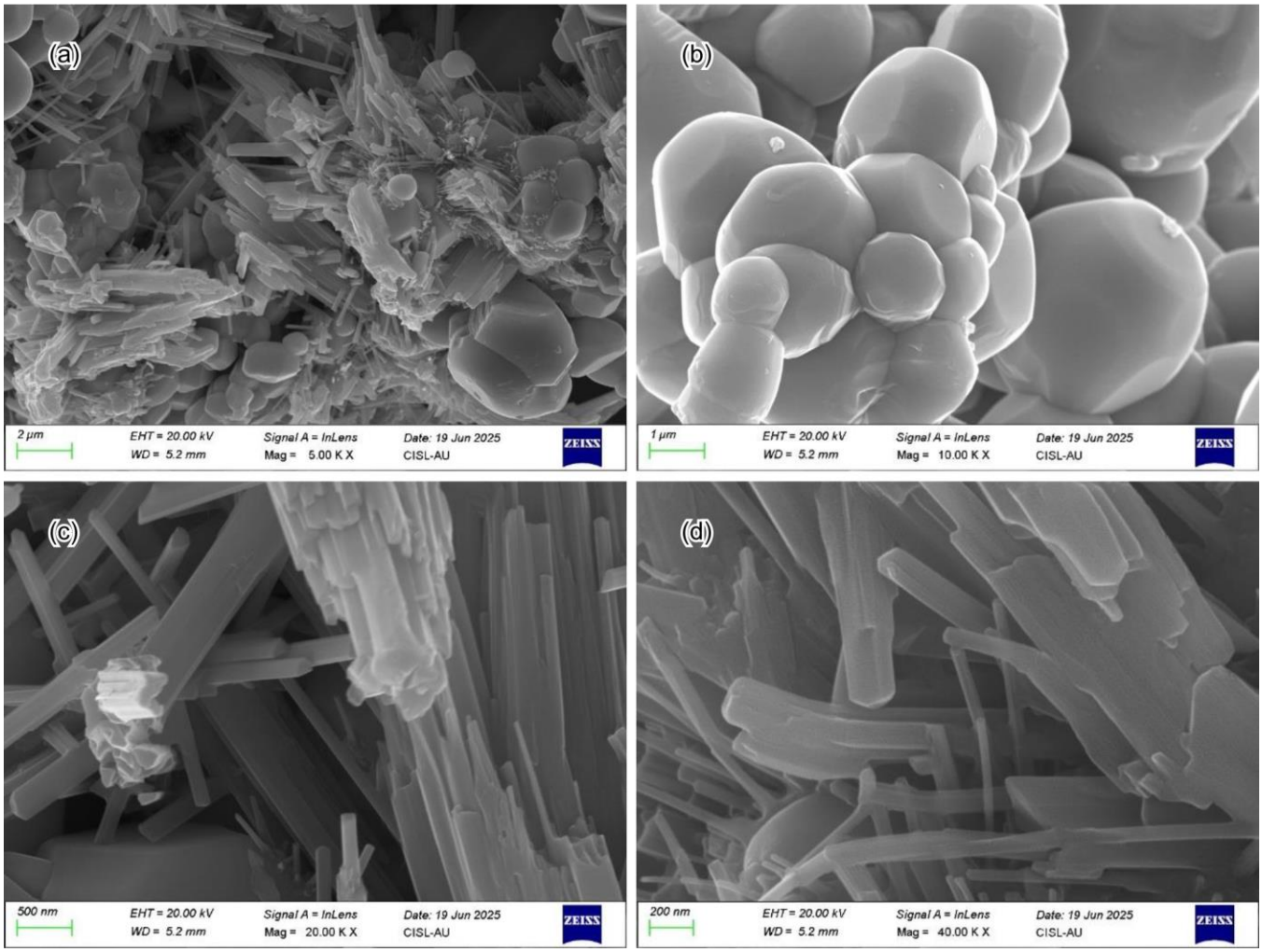

Fig. 7. FESEM images of CdSe nanorods

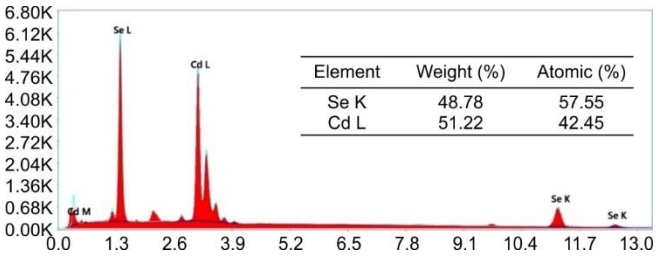

Fig. 8. EDAX spectrum of CdSe nanorods

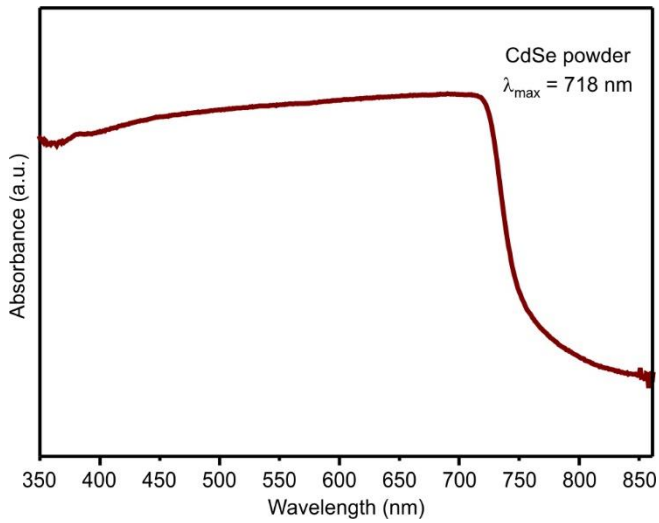

Fig. 9. UV-vis absorption spectrum of CdSe nanorods

during increased deposition time was also reported [37]. On the first view of optical microscope images, it could be seen that the particles are evenly organized and the uniformity of as-deposited film is observed at t_d =120 s. But upon increasing deposition time to t_d = 300 s, the particles were deposited on the already grown monolayer. With the increased time already deposited particles acts as activation sites for newly arriving particles which interacts with the tail of the charged layer and deposited on the top of preceding monolayer and majority of voids are filled leading to better surface coverage of the deposit.

SEM analysis of CdSe deposits: The assembly of CdSe NRs into nano-fractal array on indium tin oxide (ITO) coated glass substrate were carried out using EPD. The electric field-induced surface charge on CdSe NRs facilitates the formation of self-organized structures, as shown in Figs. 11 and 12(a-e). The deposited films were initially examined using SEM to investigate the microstructural organization and clustering behaviour of the CdSe nanoparticles. As reported in the literature [38,39], colloidal nanostructures exhibit a strong tend-

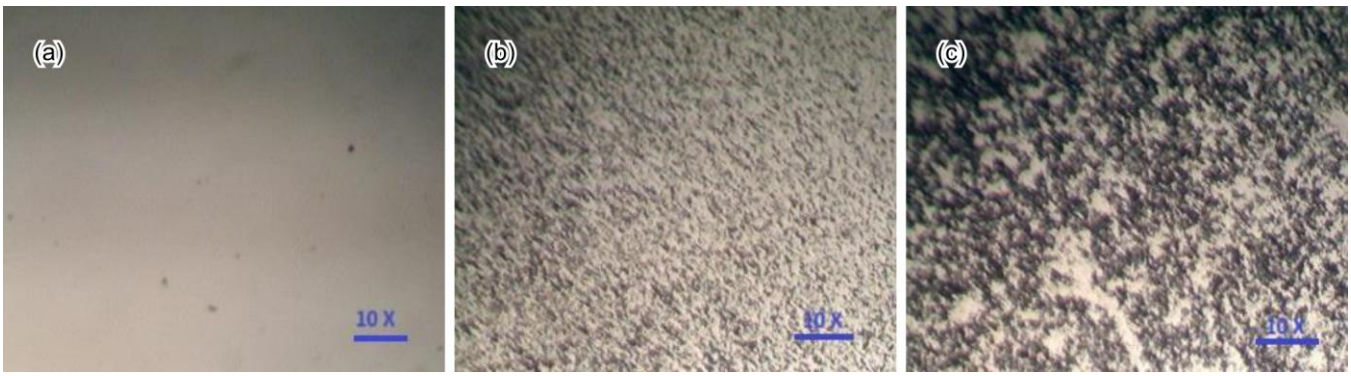

Fig. 10. Optical micrographs of (a) bare ITO, (b) t_d = 120 s, (c) t_d = 300 s

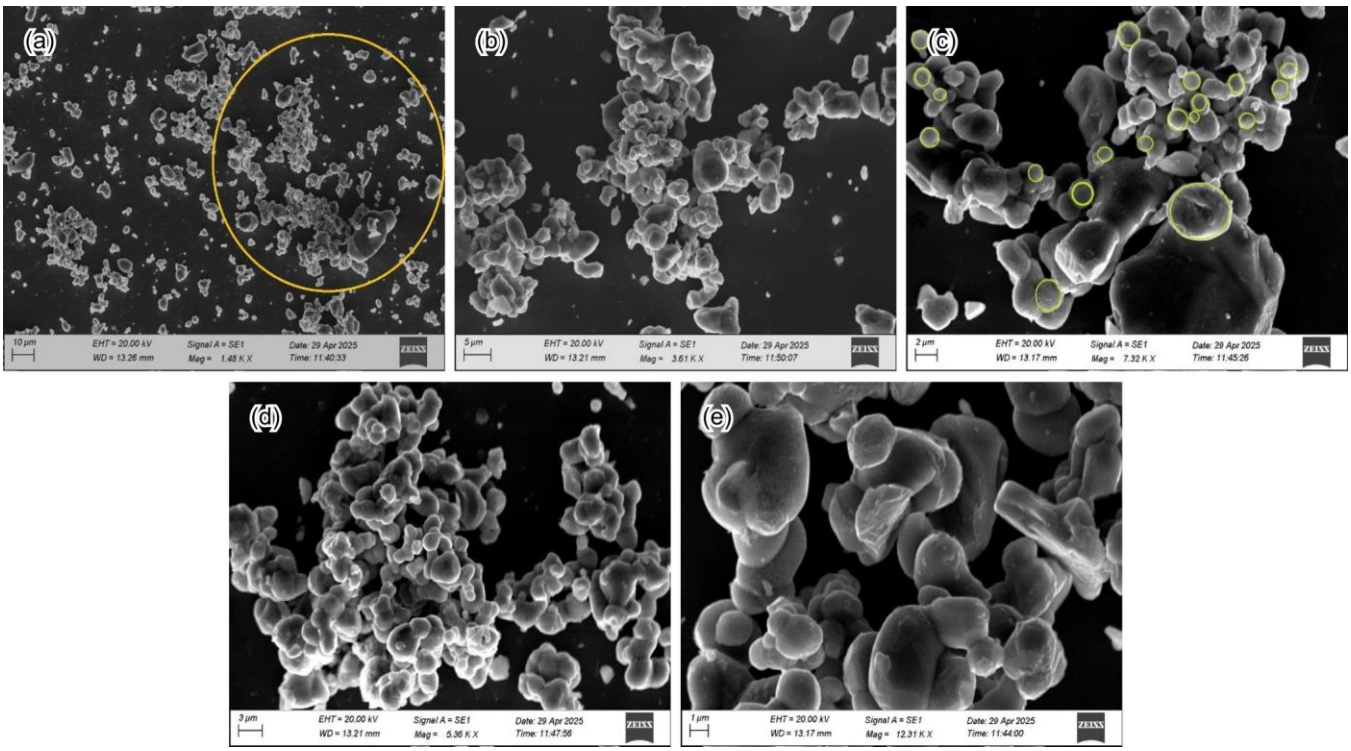

Fig. 11. SEM images of CdSe deposit at t = 120 s

ency to self-assemble into ordered arrangements such as cubic close-packed and hexagonal close-packed structures. However, these assemblies typically result in domains of limited size ranging from a few micrometers to several tens of micrometers often exhibit local structural disorder [40-43].

Under the influence of an applied electric field, nanoparticles in suspension become polarized, inducing dipole moments across individual NPs. This polarization leads to the dipole-dipole interactions, where adjacent dipoles align in a head-to-tail configuration, enhancing interparticle attractions and promoting ordered assembly [44-46]. In addition to the strengthening interparticle interactions, the external electric field also serves as a directional driving force, guiding the assembly of nanoparticles to specific regions on the substrate surface [47-50]. In the context of electrophoretic deposition, the migration of nanoparticles is governed by electrophoresis. Upon application of an electric field across the colloidal suspension, the charged nanoparticles are driven toward the oppositely charged electrode due to Coulombic forces, enabling controlled deposition of nanostructured films.

In CdSe film, under the influence of electric field, rod-like morphology seen in native powder sample Fig. 7d, is almost nullified and such CdSe-nanorods with smaller diameter remained in the colloidal suspension and particles with larger diameter (Fig. 7b) might have settled down due to larger particle size [22]. The rod-shaped particles in CdSe powder sample would have shrinked into fractal-like morphologies in CdSe film with a hexagonal pattern due to applied electric field is shown in Fig. 10a. Also, impact of electric field collapsed the microstructure and undergoes morphological deformation. As reflected in XRD results in Grazing incidence (GI) mode CdSe film has lots similarities in structural point of view. Hence, in present case, the electric field-associated assembly of nanostructures in morphological aspect could be understood, since the electric field contributes to the crystallization process in CdSe film [51].

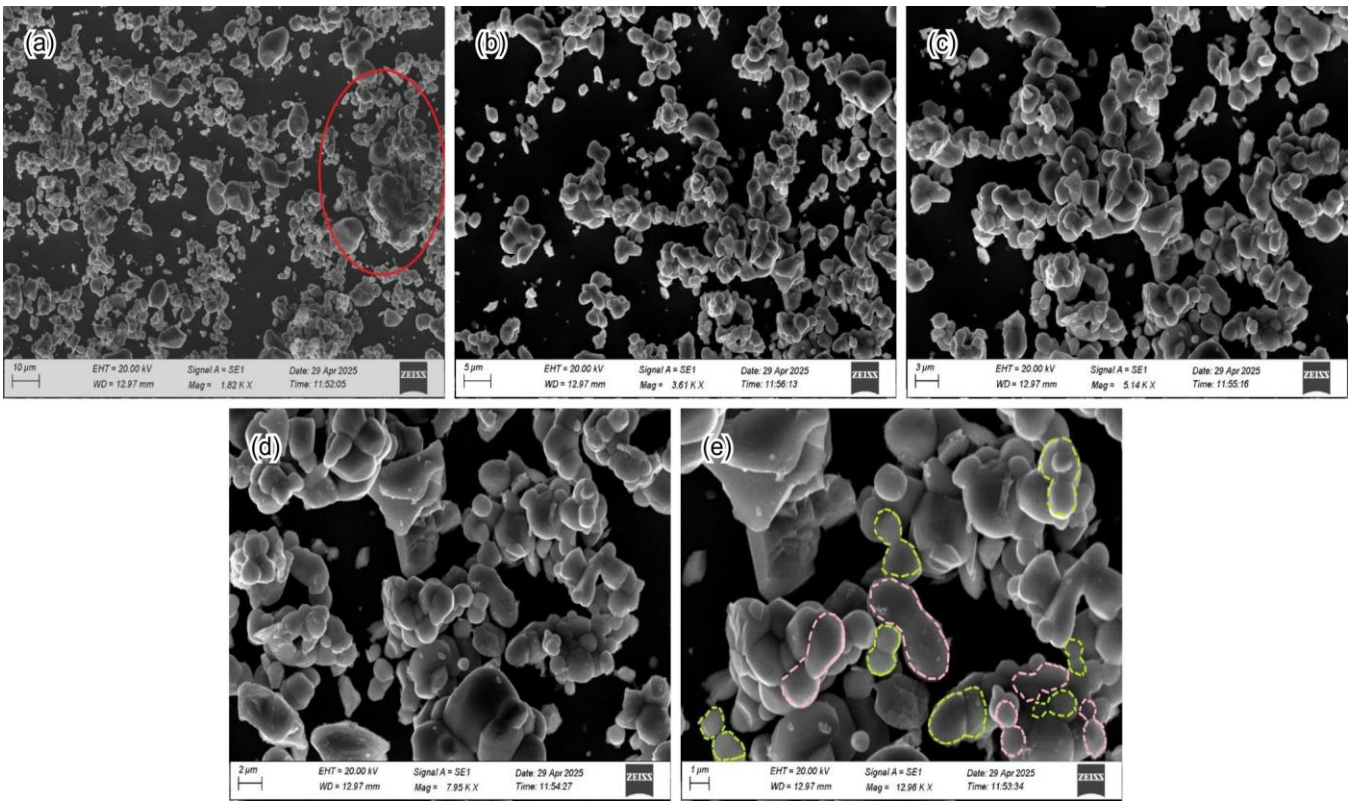

Fig. 12. SEM images of CdSe deposit at t = 300 s

For clear understanding of effect of electric field on crystallization of CdSe by EPD, the deposition voltage was fixed at 30 V and two comparative experiments were made by varying the deposition time alone at t_d = 120 s and 300 s, respectively. The surface morphology of the CdSe-deposits was obtained at different deposition duration with lower magnification is present in Figs. 10a and 11a. Interestingly, the formation of fractal like islands could be observed at t_d = 120 s. With prolonged deposition duration to t_d = 300 s, the formation of islands was further increased which explains that the particles are self-organized with effect of deposition duration (t_d). This suggests the principle behind EPD, the CdSe NRs were dispersed as individual nanorods in the colloidal suspension carrying a surface charge; during EPD it also moved under electric field as individual nanoparticles towards the electrode.

In Fig. 11a, the circled region marks the area of interest and in the context of EPD, nanoparticles in the colloidal suspension gain mobility under the applied electric field. The combined effects of fluid dynamics and the electric field distort the electric double layer (EDL), making it asymmetric thicker at the rear and thinner at the front due to electrohydrodynamic interactions. The large sized particles are existed at the right-side corner of the domains while the smaller sized and more mobile nanoscopic particles are assembled near them which reveals the arrival of nanoscopic stacked sphere-like structures near the highlighted region at 7320X magnification as displayed in Fig. 11b. Then in the vicinity of electrode, the next incoming nanrods can interact with the tail of the layer of charged nanoparticle which is close to the electrode and deposits on top of preceding nanoparticle by developing a 3D deposit. Such a clustered organization comprised of fine strips of individual particles fused together due to the shorter deposition duration of 120 s (Fig. 11c). At t_d = 300 s, the phenomena of aggregation of clusters could be seen (marked in rectangle) in Fig. 12a. During such aggregation process, the fractal like cluster islands grows in size as already stated, it rapidly grows and the distance over which it attracts newly arriving particles. It could be clearly seen that the particles approaching the cluster move towards the periphery until it reaches its favourable position, that is, a location where it may get incorporated into already existing lattice. At higher magnifications (zoom in version of rectangle shaped) at 300 s, it is interesting to observe that the irregular cavities were comprising of numerous stacked flakes like particles with smaller size shown in Fig. 12c.

The high magnification SEM images were obtained at same location of the deposits are displayed in Figs. 11 and 12(d-e). More clusters are accumulated vertically with increasing the deposition time (300 s) where surface coverage has been achieved. This explains the underlying crystallization and organizational principle of CdSe under electrophoretic deposition. For EPD of CdSe, individual particles in the colloidal suspension with nanosized regime and so the deposited films are obtained with seamless growth of larger clusters. Also, this technique appears to be field-directed self-assembly which involves the interaction of interfacial and electric potential leading to the formation of dense architectures [52].

According to such interaction, the particles got assembled on the layer adjacent to substrate surface and the film growth is observed perpendicular to the ITO substrate. Rigorous efforts have been employed for controlling the assembly of such materials with micrometer, sub-micrometre and nano-

scale patterns for variety of applications such as high-density magnetic data storage devices, biosensors, photonic materials and microchip reactors.

It is well documented that particle mobility in colloidal suspensions is primarily governed by Brownian motion, resulting in random interparticle and particle–substrate collisions [22]. The zoomed-in SEM images of the highlighted region were examined at 1230 kX magnification for deposition durations (t_d) of 120 s and 300 s. At t_d = 120 s, an assembly of similarly sized, irregular sphere-like particles was observed. Notably, at t_d = 300 s, the same region (highlighted in a red rectangle) revealed regularly stacked dumbbell-like nanostructures. These findings suggest that nanorod aggregates present in the initial CdSe powder reorganized into aligned and assembled nanostructures upon EPD.

Further SEM analysis at 3600X magnification (sample A) for t_e = 120 s revealed partially ordered spherical microstructures with occasional cavities. Prolonged deposition at t_d = 300 s led to the formation of irregular annular ring-like features with well-defined cavities approximately 300 nm in diameter. At higher magnification (5360X), semi-annular ring morphologies began to appear at 120 s but matured into more complete, space-filling voids by 300 s. This was verified by optical microscopy, indicating the formation of deposits with sufficient thickness. Elemental composition of the CdSe nanorods was examined using EDAX coupled with SEM. The spectra confirmed the presence of cadmium (Cd) and selenium (Se), along with expected signals from the ITO substrate (In, Sn, O), with no extraneous peaks indicating the high purity of the deposited CdSe film (Fig. 13).

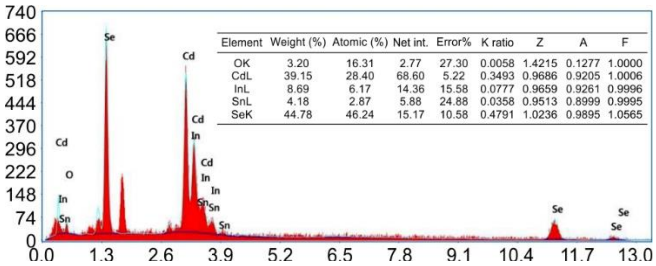

Element	Weight (%)	Atomic (%)	Net int.	Error%	K ratio	Z	A	F
OK	3.20	16.31	2.77	27.30	0.0058	1.4215	0.1277	1.0000
CdL	39.15	28.40	68.60	5.22	0.3493	0.9686	0.9205	1.0006
InL	8.69	6.17	14.36	15.58	0.0777	0.9659	0.9261	0.9996
SnL	4.18	2.87	5.88	24.88	0.0358	0.9513	0.8999	0.9995
SeK	44.78	46.24	15.17	10.58	0.4791	1.0236	0.9895	1.0565

Fig. 13. EDAX spectrum of CdSe film

High-magnification SEM images (Figs. 11 and 12d-e) revealed that particles with uniform diameters tend to form more ordered, densely packed regions compared to those with broad size distributions. The degree of ordering was found to depend strongly on deposition parameters such as applied voltage, electrode spacing, suspension concentration and especially deposition time. These results demonstrate that EPD is a promising, low-cost and eco-friendly technique for fabricating large-area, ordered CdSe nanostructured assemblies. Such organized films may exhibit tunable optical and electronic properties, making them suitable for applications in nano-optoelectronics, photovoltaics, and energy storage devices.

Conclusion

This study demonstrates the successful deposition of CdSe nanorods by EPD procedure thereby maintaining the deposition voltage at 30 V, electrode separation of 3 mm, suspension concentration as constants and varying the deposition time at 120 s and 300 s. The phenomenon of crack formation and delamination was observed and it should be observed that the nanosized dumbbell shape were stacked by enhanced deposition duration without post-heat treatment or complexating agents. The nanoparticles of CdSe with crystallite size of 76.6 nm and rods and flake-like shape having the particle diameter ranging from 30 to 50 nm was used for electrophoretic deposits of required thickness. Also, EPD is considered to be an inexpensive and pollutant free method to yield highly pure films were obtained and the crystallinity was retained. The mechanism of deposition and phenomenona of organized assembly was inferred from optical micrograph and SEM analysis of the deposits. The organized assembly of CdSe under the influence of electric field is expected to be utilized for design and fabrication of high-performance devices and sensors. The present investigation of CdSe deposited electrophoretically are suitable for the application of photovoltaic cells.

CONFLICT OF INTEREST

The authors declare that there is no conflict of interests regarding the publication of this article.

REFERENCES

1. A. Bukhtiar and B. Zou, *Mater. Adv.*, **5**, 6739 (2024); https://doi.org/10.1039/D4MA00523F
2. L.K. Li, J. Ge, E. Li, Z. Li, H. Wang, Y. Wang, Y. Zhou, and J.-J. Zhu, *EEE Catal.*, **1**, 687 (2023); https://doi.org/10.1039/D3EY00106G
3. J.H. Fendler and F.C. Meldrum, *Adv. Mater.*, **7**, 607 (1995); https://doi.org/10.1002/adma.19950070703
4. W.Z. Wang, Y. Geng, P. Yan, F.Y. Liu, Y. Xie and Y.T. Qian, *J. Am. Chem. Soc.*, **121**, 4062 (1999); https://doi.org/10.1021/ja9832414
5. J. Zhu, X. Liao, X. Zhao and J. Wang, *Mater. Lett.*, **47**, 339 (2001); https://doi.org/10.1016/S0167-577X(00)00263-9
6. S.T. Lakshmikumar and A.C. Rastogi, *Sol. Energy Mater. Sol. Cells*, **32**, 7 (1994); https://doi.org/10.1016/0927-0248(94)90251-8
7. C. Mehta, J.M. Abbas, G.S.S. Saini and S.K. Tripathi, *Chalcogenide Lett.*, **4**, 133 (2007).
8. C.A. Leatherdale, C.R. Kagan, N.Y. Morgan, S.A. Empedocles, M.A. Kastner and M.G. Bawendi, *Phys. Rev. B Condens. Matter*, **62**, 2669 (2000); https://doi.org/10.1103/PhysRevB.62.2669
9. H. Mattoussi, L.H. Radzilowski, B.O. Dabbousi, D.E. Fogg, R.R. Schrock, E.L. Thomas, M.F. Rubner and M.G. Bawendi, *J. Appl. Phys.*, **86**, 4390 (1999); https://doi.org/10.1063/1.371376
10. M.C. Schlamp, X. Peng and A.P. Alivisatos, *J. Appl. Phys.*, **82**, 5837 (1997); https://doi.org/10.1063/1.366452
11. S. Li, H. Zhao and D. Tian, *Mater. Sci. Semicond. Process.*, **16**, 149 (2013); https://doi.org/10.1016/j.mssp.2012.05.013
12. Y. Azizian-Kalandaragh and A. Khodayari, *Mater. Sci. Semicond. Process.*, **13**, 225 (2010); https://doi.org/10.1016/j.mssp.2010.10.018
13. A. Fujita, A. Ota, K. Nakamura, Y. Nabetani, T. Kato and T. Matsumoto, *Mater. Sci. Semicond. Process.*, **6**, 457 (2003); https://doi.org/10.1016/j.mssp.2003.08.006
14. S.K. Haram, B.M. Quinn and A.J. Bard, *J. Am. Chem. Soc.*, **123**, 8860 (2001); https://doi.org/10.1021/ja0158206
15. B. Vigneashwari and S.V.M. Satyanarayana, *Int. J. Nanosci.*, **10**, 1215 (2011); https://doi.org/10.1142/S0219581X11008198.

16. S. Sengupta, R. Aggarwal and M. Raula, *J. Mater. Res.*, **38**, 142 (2023); https://doi.org/10.1557/s43578-022-00539-9
17. E.T. Efaz, M.M. Rhaman, S.A. Imam, K.L. Bashar, F. Kabir, M.E. Mourtaza, S.N. Sakib and F.A. Mozahid, *Eng. Res. Express*, **3**, 032001 (2021); https://doi.org/10.1088/2631-8695/ac2353
18. B.K. Chakrabarti, M. Gençten, G. Bree, A.H. Dao, D. Mandler and C. T.J. Low, *Int. J. Energy Res.*, **46**, 13205 (2022); https://doi.org/10.1002/er.8103
19. C.P. Gutierrez, J.R. Mosley and T.C. Wallace, *J. Electrochem. Soc.*, **109**, 923 (1962); https://doi.org/10.1149/1.2425207.
20. F. Pearlstein, R. Wick and A. Gallaccio, *J. Electrochem. Soc.*, **110**, 843 (1963); https://doi.org/10.1149/1.2425882.
21. H.C. Hamaker, *Trans. Faraday Soc.*, **35**, 279 (1940); https://doi.org/10.1039/tf9403500279
22. L. Besra and M. Liu, *Prog. Mater. Sci.*, **52**, 1 (2007); https://doi.org/10.1016/j.pmatsci.2006.07.001
23. W.M. Sigmund, N.S. Bell and L. Bergström, *J. Am. Ceram. Soc.*, **83**, 1557 (2000); https://doi.org/10.1111/j.1151-2916.2000.tb01432.x
24. I. Corni, M.P. Ryan and A.R. Boccaccini, *J. Eur. Ceram. Soc.*, **28**, 1353 (2008); https://doi.org/10.1016/j.jeurceramsoc.2007.12.011
25. J. Ma and W. Cheng, *Mater. Lett.*, **56**, 721 (2002); https://doi.org/10.1016/S0167-577X(02)00602-X
26. A. Sivakumar, S.S.J. Dhas, S. Balachandar and S.A.M.B. Dhas., *J. Electron. Mater.*, **48**, 7868 (2019); https://doi.org/10.1007/s11664-019-07605-9.
27. F.-Z. Dai, B. Wen, Y. Sun, H. Xiang and Y. Zhou, *J. Mater. Sci. Amp. Technol.*, **43**, 168 (2020); https://doi.org/10.1016/j.jmst.2020.01.005
28. B. Nasiri-Tanriz, *J. Adv. Ceram.*, **3**, 31 (2014); https://doi.org/10.1007/s40145-014-0090-4
29. M. Khairy and M.A. Mousa, *J. Ovonic Res.*, **15**, 181 (2019).
30. S. Satheeskumar, V. Jeevanantham and D. Tamilselvi, *J. Ovonic Res.*, **14**, 9 (2018).
31. M.E. Fitzpatrick, A.T. Fry, P. Holdway, F.A. Kandil, J. Shackleton and L. Suominen, Measurement Good Practice Guide No.52, National Physical Laboratory (2005).
32. S. Adachi, Handbook on Physical Properties of Semiconductors, Springer (2004).
33. A.A. Saad Akl and M.M.E. Abdelbagi, *J. Ovonic Res.*, **15**, 181 (2020); https://doi.org/10.15251/JOR.2020.165.323
34. M.A. Hegazy and A.M. Abd El-Hameed, *NRIAG J. Astron. Geophys.*, **3**, 82 (2014); https://doi.org/10.1016/j.nrjag.2014.05.002
35. M. Chen and L. Gao, *J. Am. Ceram. Soc.*, **88**, 1643 (2005); https://doi.org/10.1111/j.1551-2916.2005.00267.x
36. F.I.M. Bincy, S. Oviya, R.S. Kumar, P. Kannappan, K. Jagannathan, P. Sivaprakash, I. kim and S.A.M.B. Dhas, *Materialia*, **12**, 102476 (2025); https://doi.org/10.1016/j.mtla.2025.102476
37. K.A. Yaacob and D.J. Riley, *Ceram. Int.*, **39**, 8797 (2013); https://doi.org/10.1016/j.ceramint.2013.04.067
38. R. van Dommelen, P. Fanzio and L. Sasso, *Adv. Colloid Interface Sci.*, **251**, 97 (2018); https://doi.org/10.1016/j.cis.2017.10.007
39. S.-y. Zhang, M.D. Regulacio and M.-y. Han, *Chem. Soc. Rev.*, **43**, 2301 (2014); https://doi.org/10.1039/c3cs60397k
40. T.P. Bigioni, X.-M. Lin, T.T. Nguyen, E.I. Corwin, T.A. Witten and H.M. Jaeger, *Nat. Mater.*, **5**, 265 (2006); https://doi.org/10.1038/nmat1611
41. M. Sainato, B. Shevitski, A. Sahu, J.D. Forster, S. Aloni, G. Barillaro and J.J. Urban, *ACS Omega*, **2**, 3681 (2017); https://doi.org/10.1021/acsomega.7b00433
42. X.M. Lin, H.M. Jaeger, C.M. Sorensen and K.J. Klabunde, *J. Phys. Chem. B*, **105**, 3353 (2001); https://doi.org/10.1021/jp0102062
43. N. Aubry, P. Singh, M. Janjua and S. Nudurupati, *Proc. Natl. Acad. Sci. USA*, **105**, 3711 (2008); https://doi.org/10.1073/pnas.0712392105
44. A. Azari, J.J. Crassous, A.M. Mihut, E. Bialik, P. Schurtenberger, J. Stenhammar and P. Linse, *Langmuir*, **33**, 13834 (2017); https://doi.org/10.1021/acs.langmuir.7b02040
45. S. Nojd, P.S. Mohanty, P. Bagheri, A. Yethiraj and P. Schurtenberger, *Soft Matter*, **9**, 9199 (2013); https://doi.org/10.1039/c3sm51226f
46. J. Crassous, A. Mihut, E. Wernersson, P. Pfleiderer, J. Vermant, P. Linse and P. Schurtenberger, *Nat. Commun.*, **5**, 5516 (2014); https://doi.org/10.1038/ncomms6516
47. S. Kumar, Y.K. Seo and G.H. Kim, *Appl. Phys. Lett.*, **94**, 153104 (2009); https://doi.org/10.1063/1.3118588
48. S.H. Jung, C. Chen, S.H. Cha, B. Yeom, J.H. Bahng, S. Srivastava, J. Zhu, M. Yang, S.Q. Liu and N.A. Kotov, *J. Am. Chem. Soc.*, **133**, 10688 (2011); https://doi.org/10.1021/ja200422s
49. B. Le Huy, S. Kumar and G.-H. Kim, *J. Phys. D Appl. Phys.*, **44**, 325402 (2011); https://doi.org/10.1088/0022-3727/44/32/325402
50. X.G. Xiong and A. Busnaina, *J. Nanopart. Res.*, **10**, 947 (2008); https://doi.org/10.1007/s11051-007-9351-2
51. L.F. Alexander and N. Radacsi, *CrystEngComm*, **21**, 5014 (2019); https://doi.org/10.1039/C9CE00755E
52. B. Vigneashwari, V. Ravichandran, P. Parameswaran, S. Dash and A.K. Tyagi, *J. Nanosci. Nanotechnol.*, **8**, 689 (2008); https://doi.org/10.1166/jnn.2008.A128